OAK RIDGE
NATIONAL LABORATORY
MANAGED BY UT-BATTELLE
FOR THE DEPARTMENT OF ENERGY

ORNL/TM-2011/527

STEADY-STATE COMPARISON OF GS-IHP FIELD DATA TO MODELED PERFORMANCE

January 2012

Prepared by

C. Keith Rice, Jeffrey D. Munk, Bo Shen, Richard W. Murphy, and Van D. Baxter

UT-BATTELLE
ORNL-27 (4-00)

Energy and Transportation Science Division

STEADY-STATE COMPARISON OF GS-IHP FIELD DATA TO MODELED PERFORMANCE

C. Keith Rice
Jeffrey D. Munk
Bo Shen
Richard W. Murphy
Van D. Baxter

January 2012

Prepared by
OAK RIDGE NATIONAL LABORATORY
Oak Ridge, Tennessee 37831-6283,
managed by
UT-BATTELLE, LLC
for the
U.S. DEPARTMENT OF ENERGY
under contract DE-AC05-00OR22725

CONTENTS

LIST OF FIGURES

ABSTRACT

Field tests were conducted over the winter and summer of 2011 on a prototype (ground-source integrated heat pump (GS-IHP) in Oak Ridge, TN. The extensive field test data was filtered to provide a subset of near-steady-state operation data suitable for comparison to modeled steady-state performance. On-site power use characteristics of the compressor, blower, and pumps and other operational measurements were used to calibrate the system model. Comparisons were made for four modes of operation: space heating, dedicated water heating, space cooling, and combined space cooling and water heating. Analysis results suggest that the field unit was undercharged, especially in the combined space cooling and water heating mode. The fully calibrated model agreed on average to within 2% on capacity, power, and COP/EER for the space heating and cooling modes. Average differences were larger for the water heating modes, ranging from 3 to 11%.

1. FIELD TEST UNIT DESCRIPTION

A nominal 2-ton GS-IHP is installed in a high-efficiency 3700 ft^2 home with a HERS rating of 45 for a field test in Oak Ridge, TN (Ally et al. 2011). It is connected to a horizontal loop ground heat exchanger (GHX), part of which is placed in the house foundation excavation and utility service trenches with an additional portion installed in a "rain garden" that is designed to collect rainfall runoff and keep the soil around the loop moist. The GHX loop has three parallel circuits (6 pipes) made of high density polyethylene (HDPE), with a total pipe length of 2612 ft. The loop is filled with a 20% (by volume) propylene glycol antifreeze solution (PG20). Details of the ground loop layout and the field test instrumentation and measurement accuracies have been reported previously (Ally et al. 2011).

The duct system is split into four different zones: the basement, the master bedroom, the living area, and the upstairs. The GS-IHP was programmed to control the four zone dampers (which are normally open) specifically for this installation. There are two supply ducts at intermediate locations in the house that are always open.

The GS-IHP itself uses a variable-speed compressor as well as variable-speed fan and pumps. All use brushless permanent-magnet motors. In space conditioning modes, compressor speed is controlled based on a proportional-integral-derivative controller that has the thermostat setpoints and the actual zone temperatures as control inputs. In space heating (SH) mode, the indoor blower speed is controlled to provide a minimum supply air temperature of 94°F. The ground-loop pump speed is controlled based on the entering water/brine temperature from the GHX loop.

In the dedicated water heating (WH) mode, the compressor speed is based on the entering brine temperature from the ground loop and varies over a narrower range of speeds (50 to 90 Hz) than in space heating. The required compressor speed increases as the ground loop temperature drops until the maximum allowed speed (90 Hz) is reached. In addition, the domestic hot water pump speed is controlled to maintain an 8ºF temperature rise across the refrigerant-to-water heat exchanger (HX). The ground loop pump flow is controlled based on the entering water temperature from the loop in the same manner as in space heating mode.

2. HEATING SEASON — 2011

2.1 Heating Season Field Data

Field data for the heating season was processed in a manner to enable more convenient comparisons with our steady-state Heat Pump Design Model (HPDM) predictions for the GS-IHP (Murphy et al. 2007). Because of issues with excessive unit cycling in milder heating load days due to zone air temperature sensor issues, only data from January and February were processed for use in comparison to modeled results for this report.

Due to the complexity of the GS-IHP unit, a number of onboard sensors are used to measure pressures, temperatures, and speeds in order to control the operation of the unit. ORNL was given access to collect all of the onboard sensor data in addition to our separate measurements for flow and power consumption. Owing to technical difficulties and the need for small-time-step data in troubleshooting issues with the unit, the onboard data was collected separately from the rest of the data on a laptop. This data was recorded at 4 second intervals and included all of the data

collected by the unit's control board. The rest of the data from the ORNL sensors was being recorded on a Campbell Scientific CR1000 and averaged over intervals of 1 minute and 15 minutes. Due to ongoing operational issues with the GS-IHP unit, this method of collecting data on two separate systems was maintained throughout the heating season.

In order for the data to be fully analyzed, the two data sets needed to be merged. Since the timestamps for each set of data are different, the startups of the pumps were matched with the ORNL power measurement in order to synchronize the data as well as possible. The onboard 4 second data was then averaged over 1 minute or 15 minute intervals depending on which data set it was going to be matched with from the CR1000 data logger. Since the GS-IHP simulation model is only intended for steady-state analysis, all data from startup periods were removed.

The first step taken in our equipment performance comparisons was to compare the initially assumed power versus flow curves to those measured in the field for the blower and two pumps. Field pump and blower power data were plotted over a wide range of flows and compared with the default model predictions. The uncertainty in the power measurements was 1.1%. (An uncertainty analysis on the measurements recorded by researchers is given in Appendix A.)

2.1.1 Blower Power Comparison

The original modeling of a GS-IHP for TRNSYS annual performance simulations conducted in early 2011 (Rice, Shen, and Monk 2011) used models of blower and pump power vs. flow based on assumptions of external static pressure (ESP) and water loop system heads at nominal flow rates.

For the blower, this assumption was 0.5 in. water ESP at 790 cfm. Based on the ECM blower lab tests at this nominal flow and ESP, we estimated a blower power vs. flow curve at higher and lower flow rates, assuming that the power varied with the airflow (SCFM) to the 2.7 power.

In the field test of the GS-IHP with zoned damper control, the duct system had a varying duct system resistance depending on the number of dampers which were closed. However, since two supply ducts were always open, the blower power levels between only one and all controlled dampers open were found to group approximately into two curves. This can be seen in Figure 1 where field tests were conducted (in blower only operation) while measuring the blower power over the full range of allowed airflows from 400 to 1000 cfm. These tests were run over a range of zoned dampers open as shown in the plot legend. (Note that the dampers are either fully open or closed.)

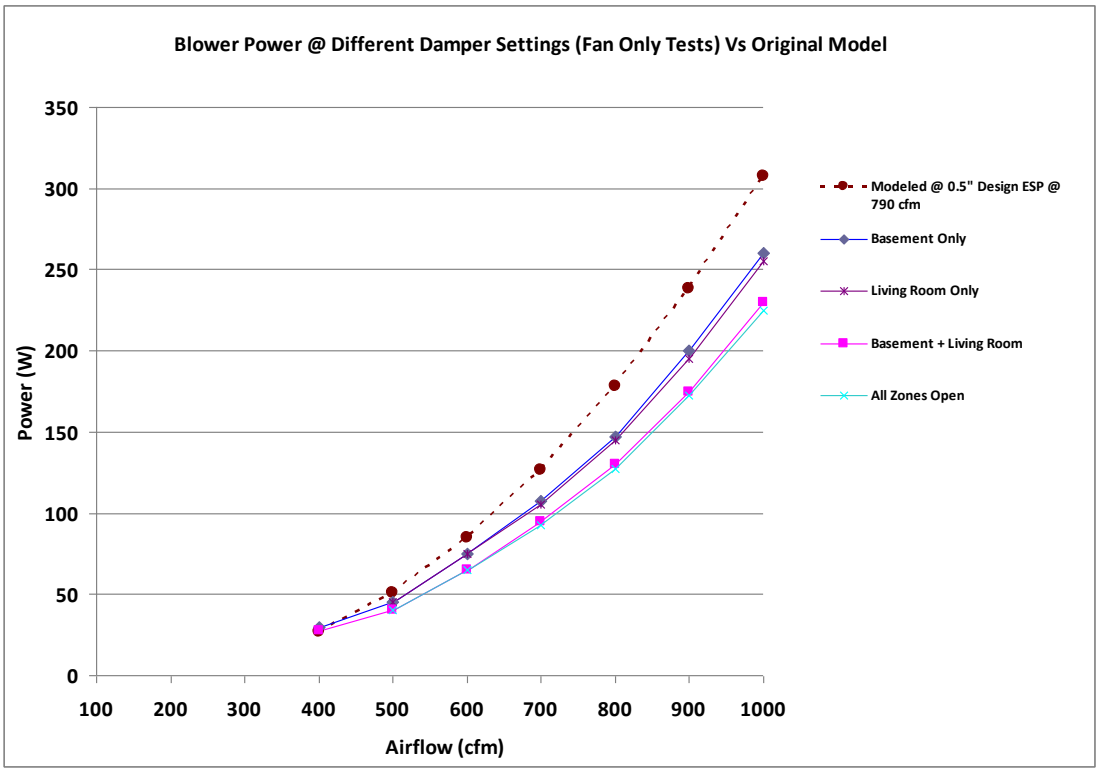

Figure 1. Modeled and field blower powers versus airflow.

In general, the power trends with flow in the field tests follow the general shape of the originally modeled curve but are 19 to 29% lower at the nominal flow rate of 790 cfm. Field-measured ESPs at the nominal flow rate were 0.25 in. and 0.11 in. for the higher and lower field blower power curves, respectively. This is consistent relative to the higher modeled power at 0.5 in. ESP, since the indoor air handler also contributes a significant fixed amount to the total static seen by the blower at nominal flow rate.

To more closely model the blower power with the lower field ESPs, quadratic curve fits of power vs. flow were made for the higher and lower field curves for use in new system model performance comparisons.

2.1.2 Domestic Hot Water Pump Power Comparison

For the domestic hot water (DHW) loop, we originally assumed a nominal system head of 7 ft of water at 4 gpm based on the pressure drop in the DHW refrigerant-to-water HX and an assumed 25 ft of ¾ in. cross-linked polyethylene PEX tubing. This is shown as the lowest dotted line in Figure 2 based on the original system head assumptions as applied to the variable-speed DHW pump performance curves. The field-measured pump power, shown as the solid curve in Figure 2, for an average circulating DHW temperature of approximately 113°F, is seen to be quite a bit larger than the originally modeled power.

In contrast to the blower situation, the DHW loop has higher system pressure drop than assumed. The higher dotted curve in Figure 2 shows the predicted power level with the system head increased by a factor of 1.9. This curve is much closer in agreement, indicating that the actual

system loop pressure drop in the field setup is about 2 times larger than the original assumption. This is believed to be due to the added pressure drop from the in-line turbine meter for our flow measurement, added resistance from thermocouple wells and other reducing fittings, and approximately 50 ft of PEX tubing.

As in the case for the blower, quadratic curve fits of power versus flow were made for the field data for use in the revised system model performance comparisons.

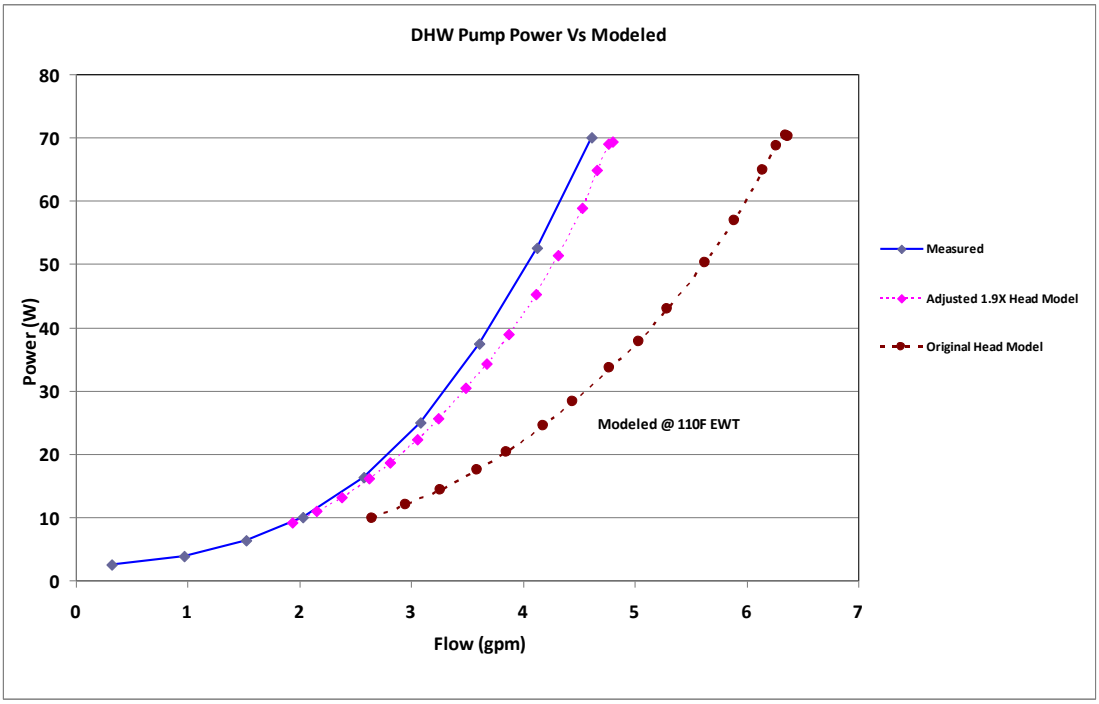

Figure 2. Modeled and field DHW pump powers versus water flow.

2.1.3 Brine Loop Pump Power Comparison

For the ground loop (brine) pump using PG20, the original system loop was assumed to be two parallel vertical bores 200 ft deep, with nominal ¾ in. diameter HDPE U-tubes (total of 800 ft of HDPE in the two bores). This gave a nominal total system head of 27.5 ft of water at 7.9 gpm. In contrast, House 2 has three parallel horizontal circuits of ¾ in. HDPE tubing of total length 2610 ft, also using PG20 brine; measured total system head was not available.

The brine pump was tested over a flow range from 1.1 to 8.4 gpm with an average brine temperature of 78°F. A comparison between the initially modeled and measured brine pump power as a function of brine flow rate is shown in Figure 3. These curves were surprisingly close in both values and trend with flow rate considering the different application assumptions. As for the blower and DHW pump, quadratic curve fits of power versus flow were made for the field data for use in the revised system model performance comparisons.

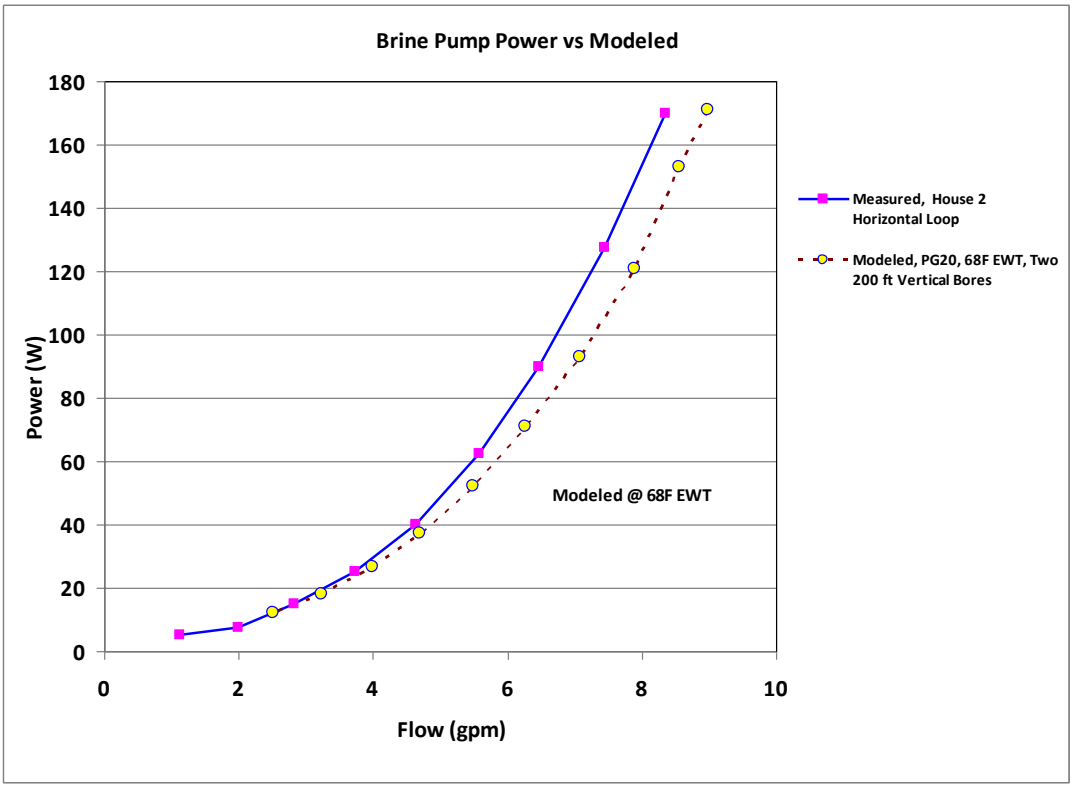

Figure 3. Modeled and field brine pump powers versus brine flow.

2.1.4 Compressor Power Correction Factors for Heating Season Operation

We compared the measured 15-min average compressor power to that predicted by the compressor map at the same compressor speed and measured suction conditions and discharge pressure. These comparisons were used to develop compressor power correction curves as functions of compressor speed and brine loop entering water temperature (EWT) for the SH mode and also a function of DHW EWT (also denoted as EHWT) for the WH mode. The field-based power adjustment factor curves for selected brine and DHW EWTs follow for space and water heating modes, respectively. (The EWT dependence for the WH mode was somewhat weaker than the EHWT effect over the tested temperature ranges.)

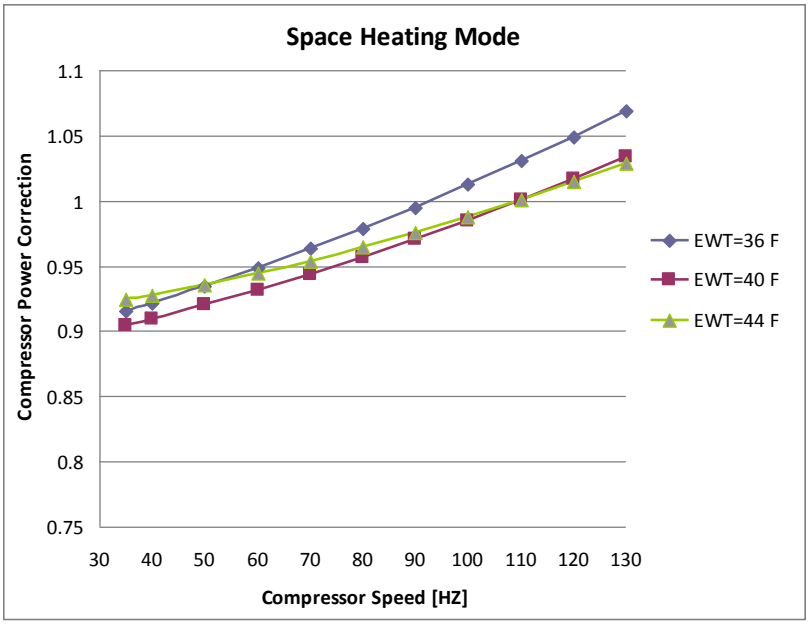

Figure 4. Compressor power correction factors for space heating mode as a function of compressor speed and EWT.

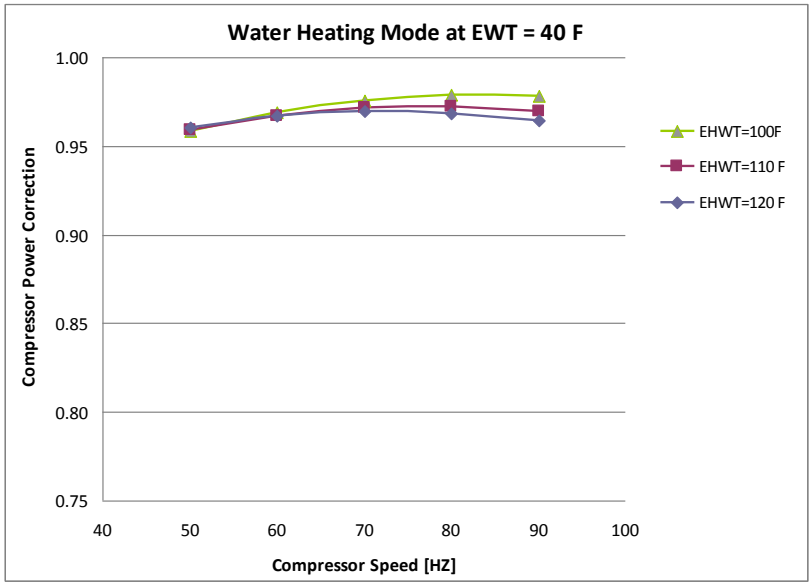

Figure 5. Compressor power correction factors for water heating mode as a function of compressor speed and EHWT for EWT = 40ºF.

The power multipliers below 1.0, especially in the space heating mode, suggest that the inverter used in the field test unit may have been operating more efficiently at lower speeds than the one in the compressor map testing. The suction-gas-cooled heat sink on the inverter in the field unit may have contributed to this improved efficiency.

2.2 Performance Comparisons for Space Heating Mode

Once the field blower and pump power versus flow characteristics were accounted for, we proceeded with HPDM simulations of our lab-data-calibrated GS-IHP model in the space heating mode. For this comparative analysis, we used 15 min average field data for return air dry-bulb (DB) temperature, brine EWT, and compressor speed as inputs to drive the HPDM model. Initial performance comparisons were made with flow power adjustments included. A 5% compressor mass flow rate derating was also initially applied based on lab-test results since refrigerant flow rate was not measured in the field test. The initial comparisons with field data for space heating capacity as a function of compressor speed are shown in Figure 6. The average brine and return air temperatures for all the pseudo-steady-state field data are noted on the plot.

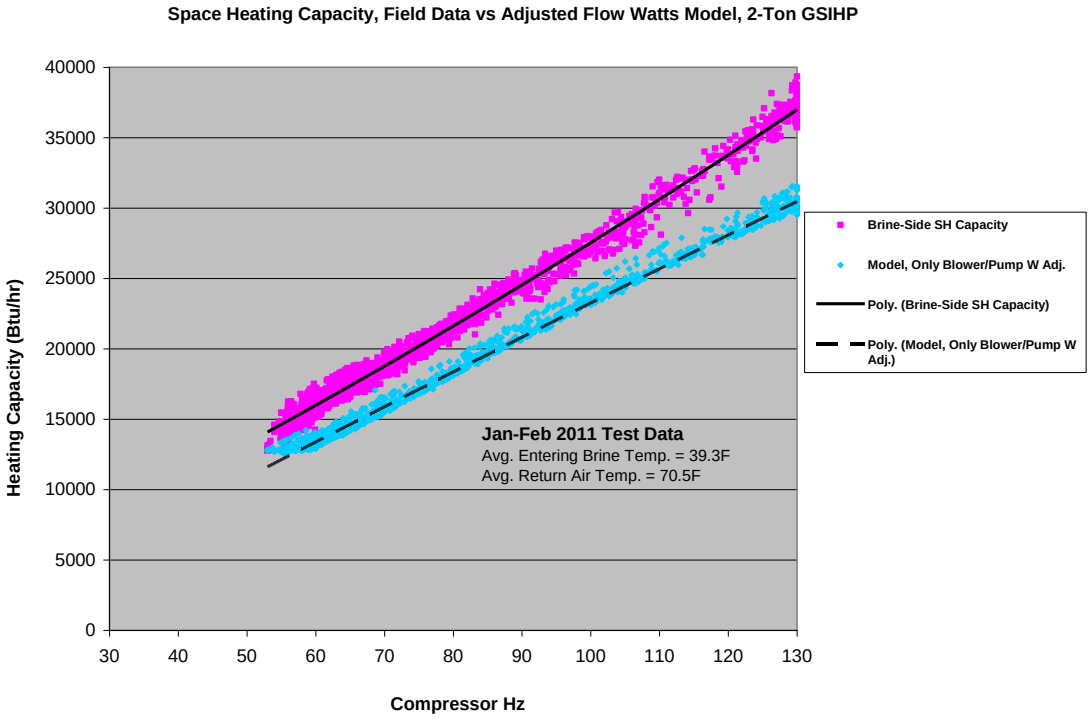

Figure 6. Comparison of initially modeled versus field space heating capacities versus compressor speed.

The modeled capacity results are seen to be lower than the field values derived from the brine-side capacity and the measured total power input. The average under-prediction is 15%.

Next a series of further adjustments were made to the modeling assumptions to better match field conditions. These included:

1) dropping the 5% compressor map flow derating based on lab tests,
2) reducing refrigerant charge to better match lower levels of measured condenser subcooling,
3) reducing discharge line heat losses,
4) using average return air temp from all zones rather than the central t-stat temperature,
5) including all system heat losses as delivered capacity (compressor shell heat loss, line heat losses, control power) consistent with the field data reduction analysis, and

6) using field-indicated indoor airflow rates rather than model-predicted to provide 94°F supply air temperatures.

Because there were no direct measurements of refrigerant mass flow rate in the field tests, we decided to revert to the uncorrected compressor manufacturer's mass flow data rather than use the 5% lower values derived from lab test data, based on an overall system energy balance, for a different compressor (of the same model).

2.2.1 Indoor Airflow Comparisons

Figure 7 shows a comparison of the original model-determined airflows versus those indicated from the field data. The airflow control approach in the space heating mode is to maintain a supply air temperature of 94°F up to a maximum airflow of 1000 cfm. It can be seen that the indicated field airflows are somewhat higher than the predicted values. A revised comparison was made after applying only adjustments 1–5 above and again predicting the airflow rates, with only slight improvement in airflow agreement. For whatever reason, the indicated field airflows do not match up closely with the predicted values. Note especially that the maximum airflow level is reached at lower compressor speeds than modeled.

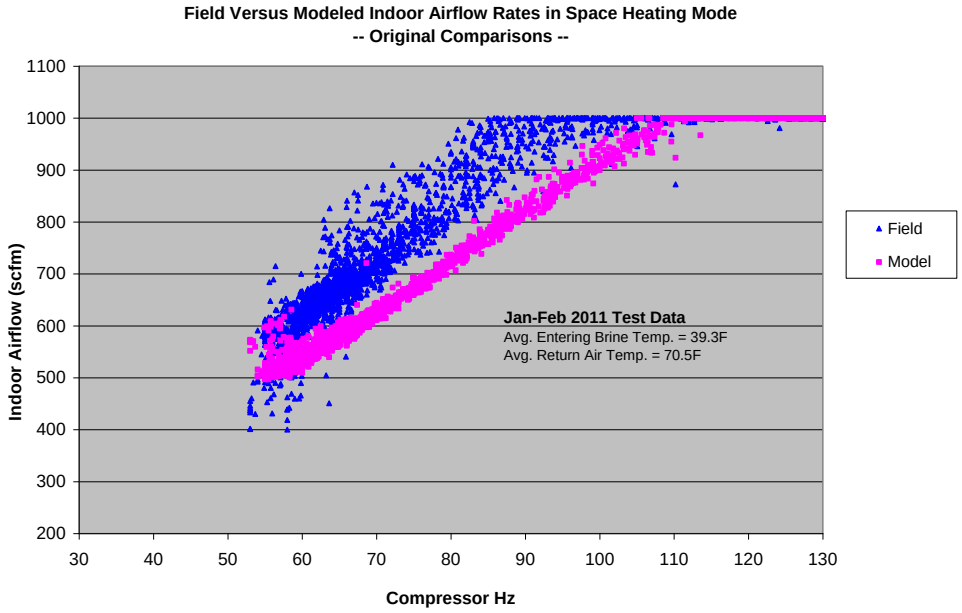

Figure 7. Comparison of field and modeled indoor airflows versus compressor speed.

One hypothesis is that the field sensor used to measure the supply air temperature is being affected by radiation from the condenser coil and thus reading a higher exit air temperature than is being delivered. Figure 8 shows a comparison of the originally modeled versus field-indicated leaving (supply) air temperatures. One can see that the target leaving temperature of 94°F is met in the modeled results at higher compressor speeds up to 110 Hz, while the field data starts to exceed the target temperature more consistently above 90 Hz operation. This is consistent with the field unit operating at higher airflows to reach the indicated supply temperature, thereby reaching the maximum airflow of 1000 cfm at a lower compressor speed. At higher compressor speeds, the measured supply temperatures will accordingly increase above the target temperature sooner and to a higher end point than for the modeled case.

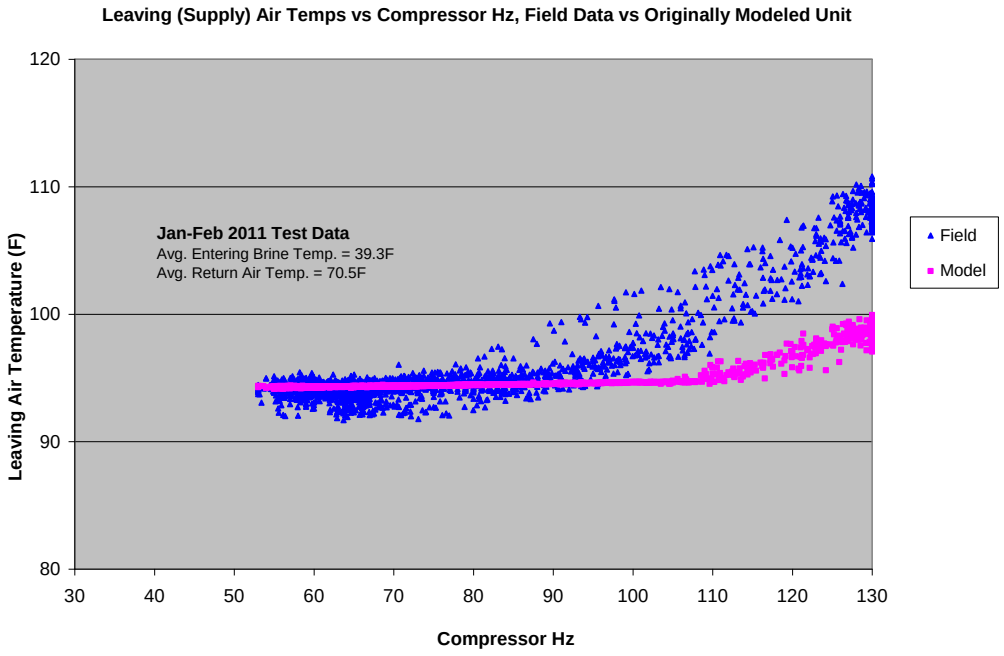

Figure 8. Comparison of field and modeled indoor air supply temperatures versus compressor speed.

For the performance comparisons that follow, we used the field-indicated indoor airflows to generate the modeled results. New comparisons for space heating capacity with this "fully adjusted" model are shown in Figure 9. The average agreement is now –0.7 %.

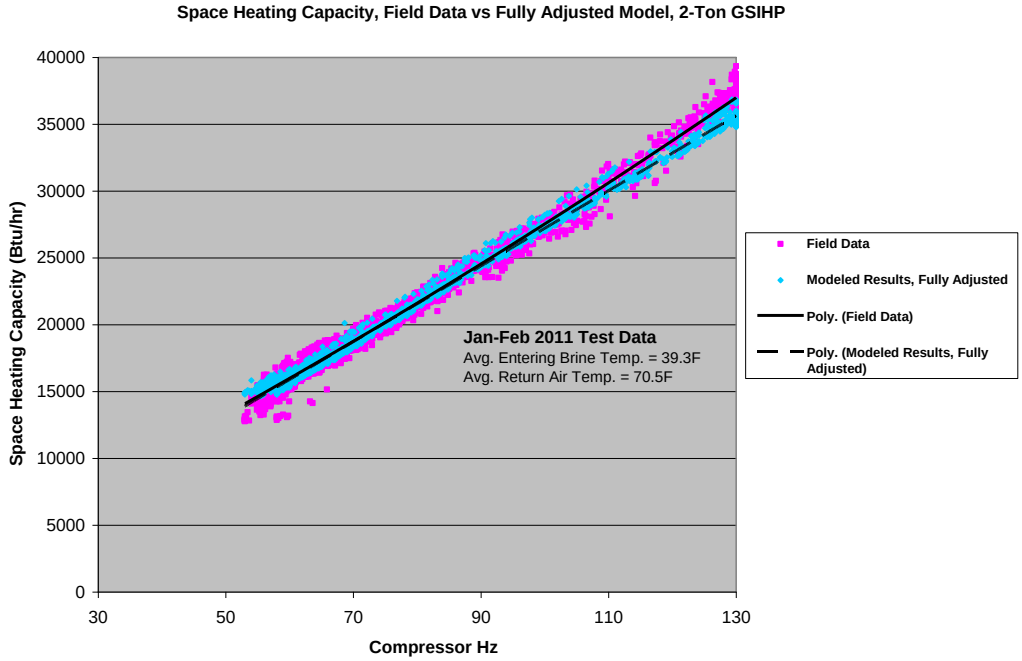

Figure 9. Space heating capacity comparison between fully adjusted model and field versus compressor speed.

While the heating capacity agreements are close for the fully adjusted model, the leaving air temperatures are still lower than the measured values. This is shown in Figure 10, where even when using the indicated airflows, there is a consistent under-prediction except for some cases where the indicated airflows dropped quite low below 65 Hz (as can be seen in Figure 7). One possible reason for this continued difference is that some of the compressor and control heat may be adding to the supply air temperature, while this was not assumed in the model. This heat was assumed to be rejected to the indoor space as delivered capacity but was not added to the supply air.

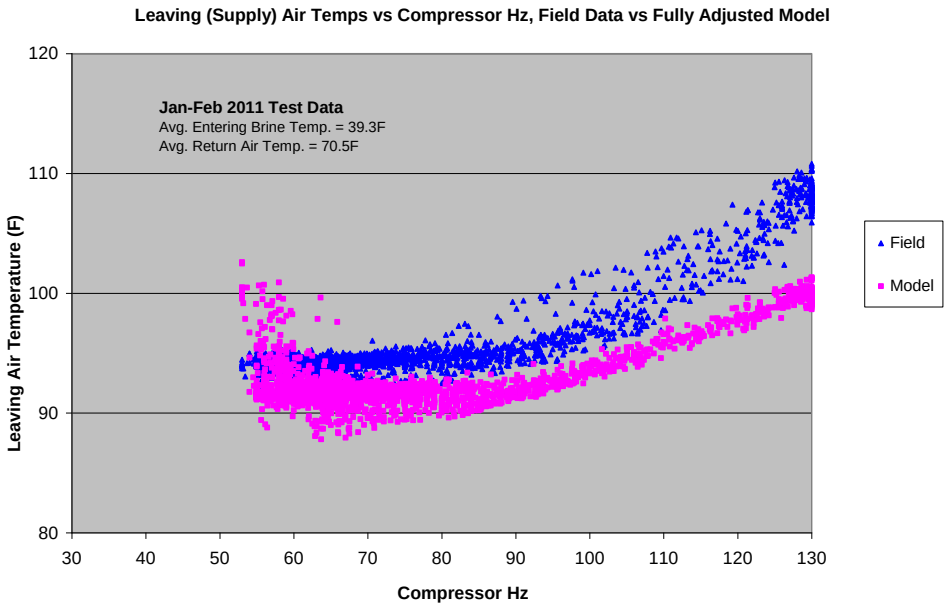

Figure 10. Comparison of field and modeled indoor air supply temperatures versus compressor speed for the fully adjusted model.

Next, the predicted power draws are compared with the field data. This is shown in Figure 11.

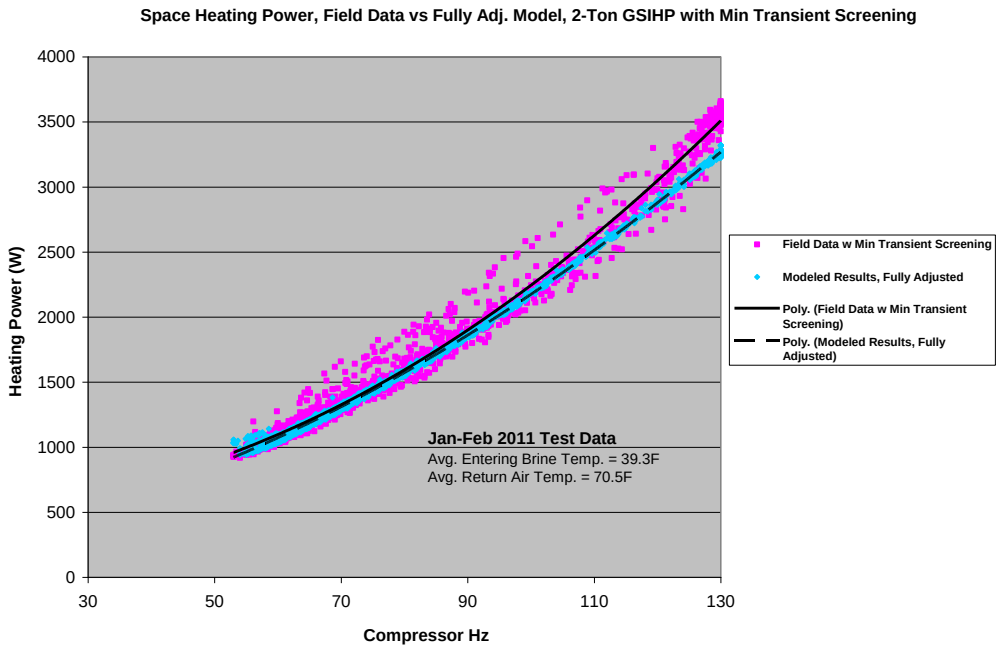

Figure 11. Space heating power comparison between fully adjusted model and field data versus compressor speed — minimum transient screening.

It is immediately seen that the power comparisons have a somewhat wider scatter than the heating capacity values. This is apparently because the calculated heating capacity values (based on brine capacity plus power draws) are damped by the slower brine capacity response. Even so, the average difference is only –2.3%.

Next, additional screening was applied to the field data to remove 15 min average data points with more transient aspects. These include those data:

1) with no compressor activity in the previous 15 minutes and
2) where the compressor speed increased or decreased by more than 10 Hz.

We term this data treatment as maximum transient screening. The effect of this screening is shown in Figure 12 where the scatter is considerably reduced and the average agreement improves to –1.6%.

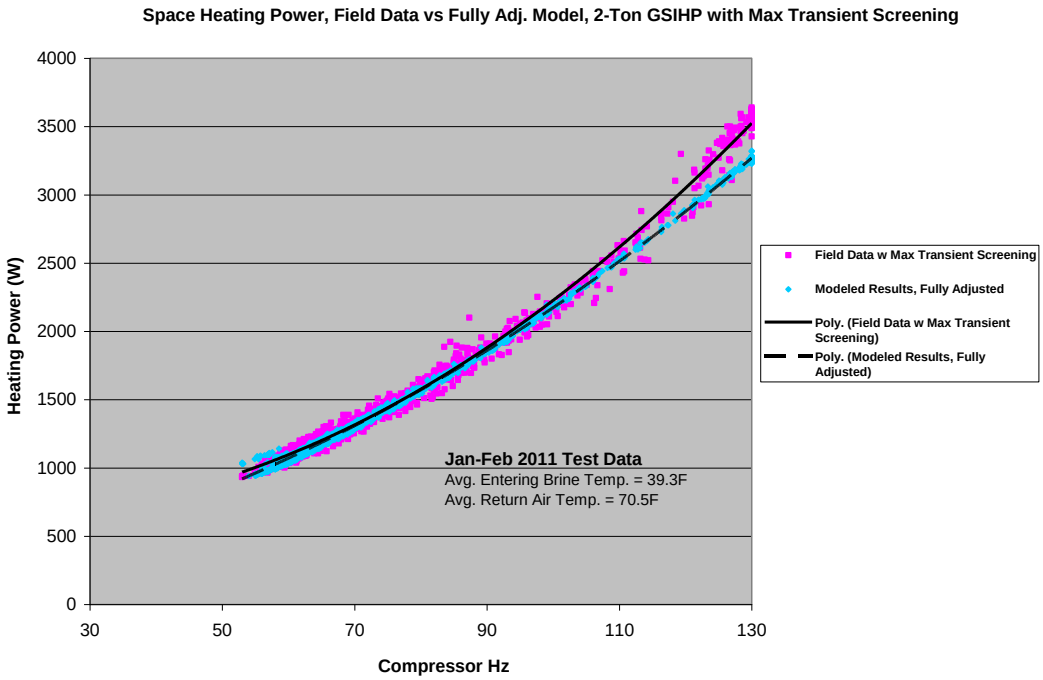

Figure 12. Space heating power comparison between fully adjusted model and field data versus compressor speed — maximum transient screening.

Next comparisons of space heating COP are shown in Figure 13 for the fully adjusted model, but with minimal transient screening. This shows a fairly larger scatter in the field-based COP values. However the average agreement is 1.7%, since the power under-prediction is more than the capacity under-prediction.

The transient data with the most deviation in agreement was for cases where the compressor speed had dropped more than 10 Hz in a 15 minute period, somewhat more so than for cases where the speed increased more than 10 Hz. This is most likely because the compressor speed has been generally observed to drop more quickly than increase. However, in both cases, it takes some time for the system to reach steady-state conditions at the new speeds. This is thought to be due to thermal inertia effects in the heat exchangers.

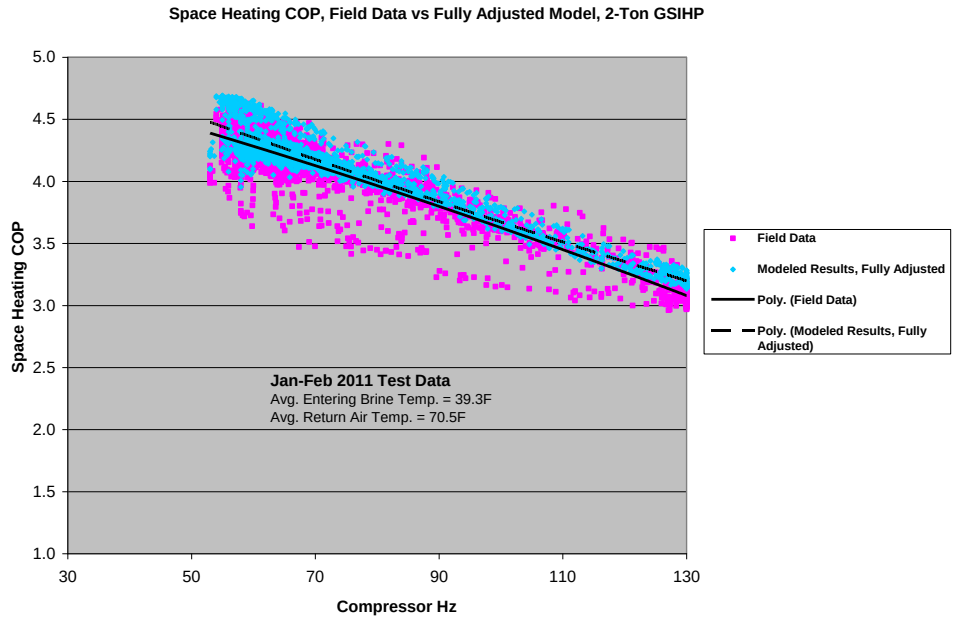

Figure 13. Space heating COP comparisons between fully adjusted model and field data versus compressor speed — minimal transient data screening.

In Figure 14, comparisons of space heating COP are shown for the fully adjusted model with maximum transient screening. Here, as for the power comparisons, the scatter in the field COP values is much reduced with agreement improved to an average of 1.1%.

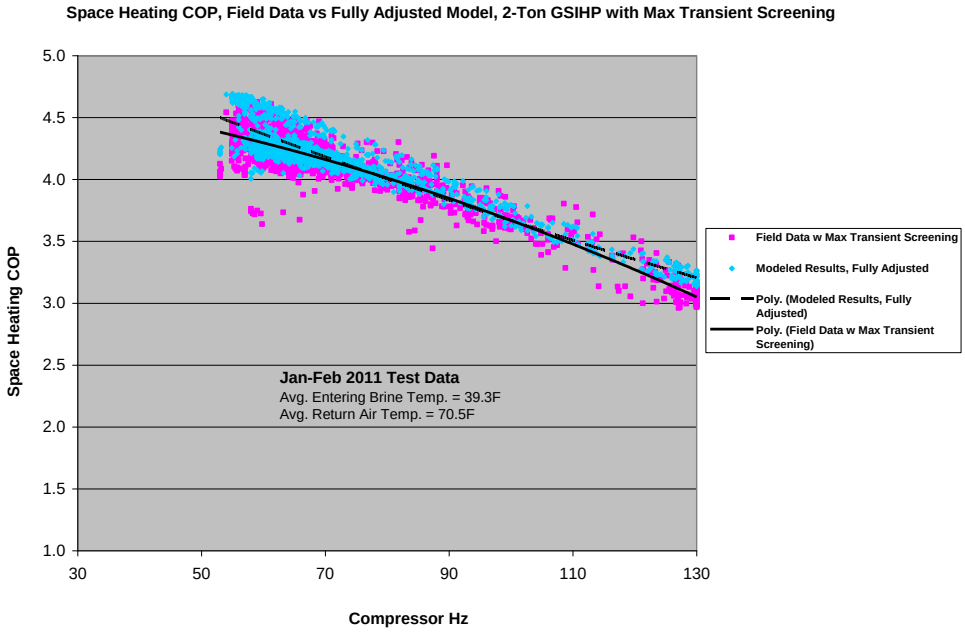

Figure 14. Space heating COP comparisons between fully adjusted model and field data versus compressor speed -- maximum transient data screening.

2.3 Performance Comparisons for Dedicated Water Heating Mode

Next, water heating simulations were conducted using the 15 minute averaged compressor speeds and brine and DHW loop EWTs as model inputs. Here adjustments were needed to match the measured DHW loop flow rates which were being controlled to maintain an indicated 8ºF water delta-T across the HX. Further adjustments were also needed to match the measured compressor discharge temperatures and condenser exit subcooling levels.

Once the various adjustments were made to obtain closer matches with the observed field component conditions, comparisons of water heating capacity and COP were made. These are shown in the following plots of figs. 15-17 as a function of DHW loop EWT along with the average compressor speed and brine EWT. (The water heating set point was 120°F.) Average differences in predicted water heating capacity, power, and COP were –1.3, –3.5, and 2.3%, respectively. These agreements indicate that the measured water heating performance levels are consistent with the observed flow and operating state conditions. However, as for the space heating mode, the indicated subcooling levels were lower than those found to give better performance in lab tests of the prototype. This suggests that the refrigerant charge was lower than optimal for this unit.

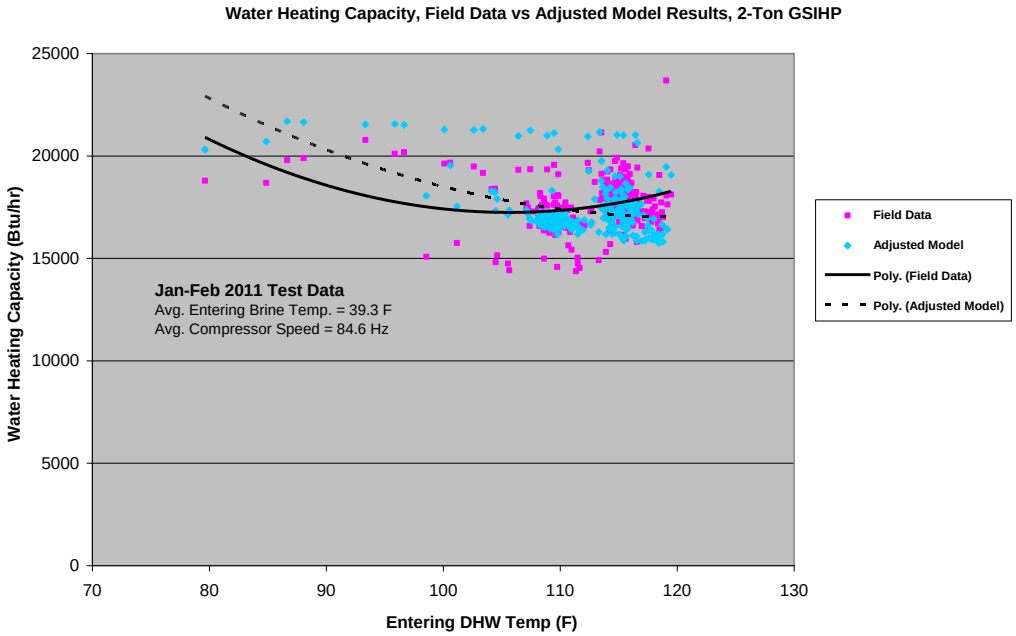

Figure 15. Dedicated water heating capacity comparison between fully adjusted model and field data over tested entering DHW temperature range.

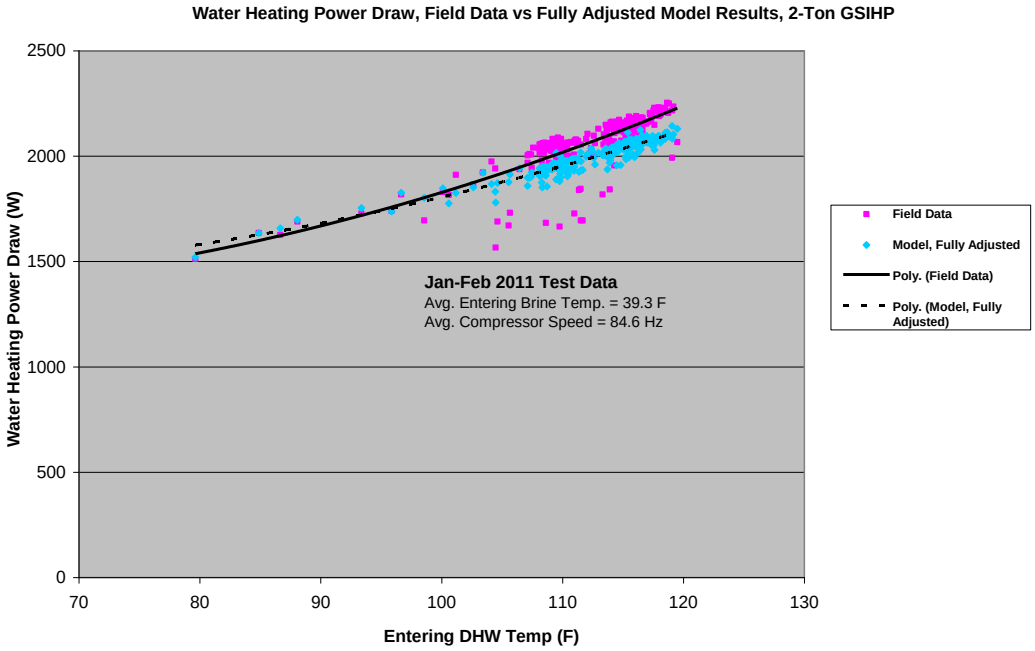

Figure 16. Dedicated water heating power comparison between fully adjusted model and field data over tested entering DHW temperature range.

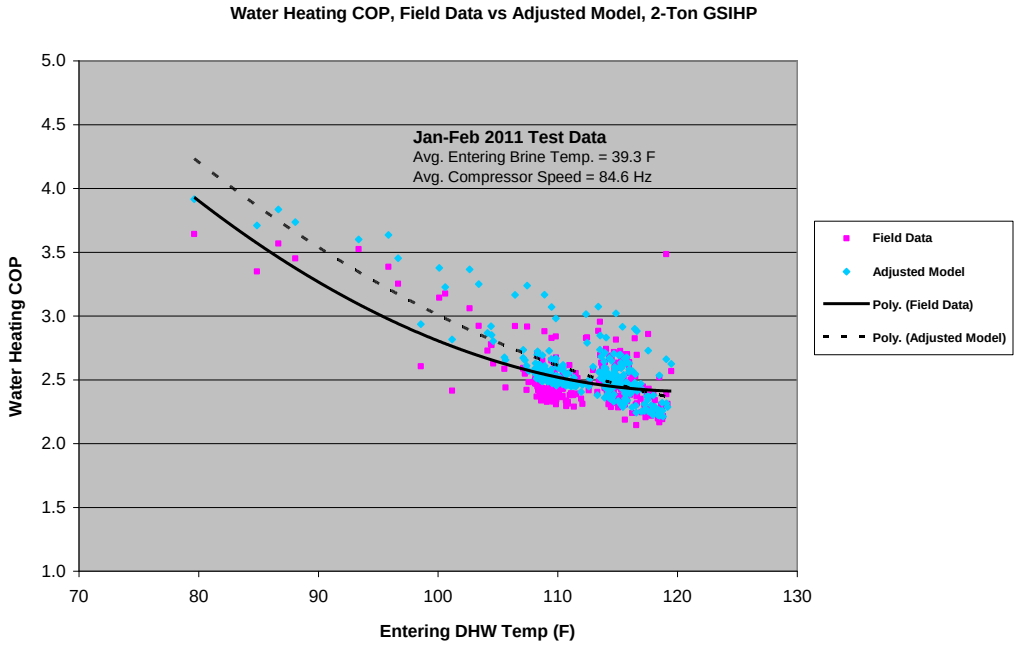

Figure 17. Dedicated water heating COP comparison between fully adjusted model and field data over tested entering DHW temperature range.

3. COOLING SEASON — 2011

3.1 Cooling Season Field Data

Field data for the cooling season operation of the GS-IHP was processed in a similar manner to that in heating mode, again to facilitate more convenient comparisons with our steady-state HPDM predictions for the GS-IHP. In contrast to the heating-mode-data issues for the milder parts of the season, data from late April to the end of September 2011 were processed for use in comparison to modeled results.

The data were separated by mode between space cooling (SC) and combined space cooling and water heating (SC+WH) and averaged over 10 minutes. (There was minimal dedicated water heating in this test period.) For both modes, the compressor speed was determined by the departure of the average indoor DB temperature from the indoor set point of 76°F (per Building America protocol), with limits on low and high speed operation in the combined SC+WH mode. Here, as in the dedicated WH mode, the minimum allowed compressor speed was 50 Hz, rather than the 40 Hz minimum in SC alone, while the maximum WH speed was again 90 Hz.

3.1.1 Compressor Power Correction Factors for Cooling Season Operation

We first compared the measured 10 minute average compressor power to that predicted by the compressor map at the same compressor speed, suction conditions, and discharge pressure. This was used to develop compressor power correction curves as functions of compressor speed and brine loop EWT or DHW EWT, for SC and SC+WH modes, respectively. These corrections are shown in figures 18 and 19.

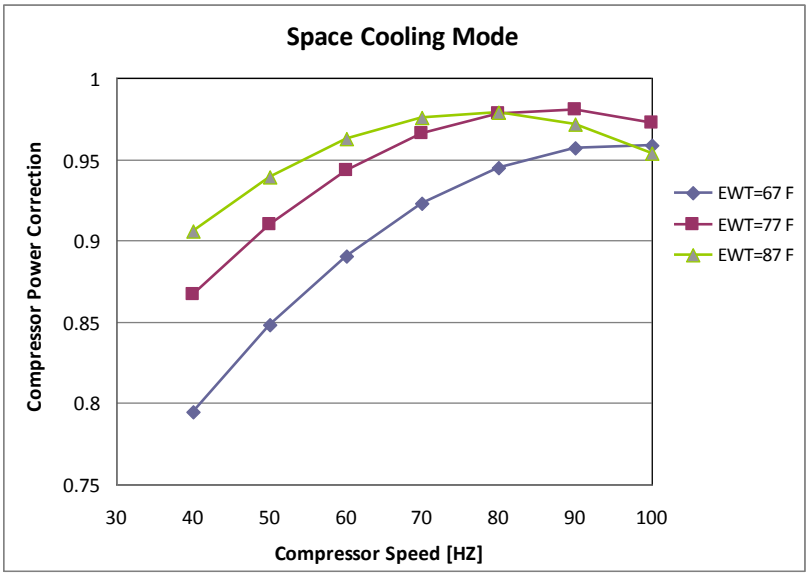

Figure 18. Compressor power correction factors for space cooling mode as a function of compressor speed and EWT.

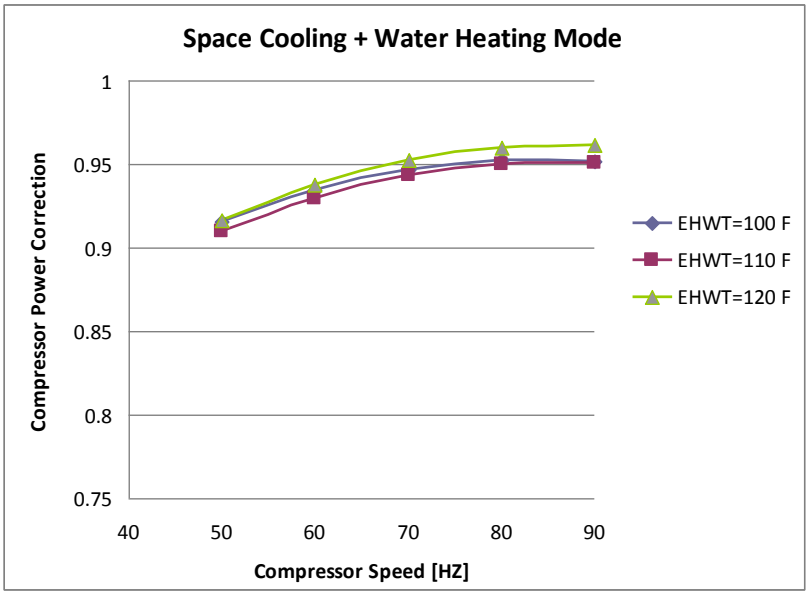

Figure 19. Compressor power correction factors for SC+WH mode as a function of compressor speed and EHWT.

As in space heating, the power multipliers below 1.0, especially in the space cooling mode, suggest that the inverter used in the field test unit may have been operating more efficiently at lower speeds than the setup in the compressor map testing. The suction-gas-cooled heat sink on the inverter may have contributed to this improved efficiency. Note also that the compressor map only has test points down to 90ºF condensing temperature, so extrapolation errors from the map curve fits may account for the larger needed corrections at lower EWTs (below 77ºF EWT at lower compressor speeds). As in space and water heating modes, no corrections were made to the map-predicted compressor mass flow rates, as refrigerant flow was not measured in the field tests.

3.2 Performance Comparisons for Space Cooling Mode

Using the 10-minute averages for measured

1) compressor speed,
2) indoor airflow rate,
3) indoor DB and relative humidity (RH),
4) entering brine or DHW temperatures, and
5) indicated condenser subcooling, evaporator superheat, and compressor discharge temperatures,

the HPDM was run to obtain simulated power, capacity, and EERs in the space cooling mode. We used a curve of indoor blower power versus flow slightly modified from that used in heating mode and based on field data, to account for the additional wet coil pressure drop. Since most of the cooling mode operation was with the dampers for the living room and the basement open, we only used a single modified curve for the less restrictive duct system. We also added to the modeled indoor unit capacity all the heat losses from the components and control system that end up as heat delivered to the indoor space, as were included in the field capacity values.

Figures 20-23 show the resultant comparisons of space cooling capacity, total power, and EER between field data and modeled results as a function of compressor speed. The average return air temperature and RH and entering brine temperature for all the space cooling mode data are noted in the plots. In contrast to the quite narrow range of entering brine temperatures in the heating mode (~37 to 46ºF) the brine temperature varied over a rather wide range for the April–August cooling season data (from ~55 to 90ºF). This wide variation accounts in large part for the scatter seen in the performance results when plotted only as a function of the compressor speed.

The average differences in space cooling capacity, power, and EER between the field and modeled values are –0.5%, –0.1%, and –0.4%, respectively. Note also that the RH control was excellent with an average RH of 48.2%.

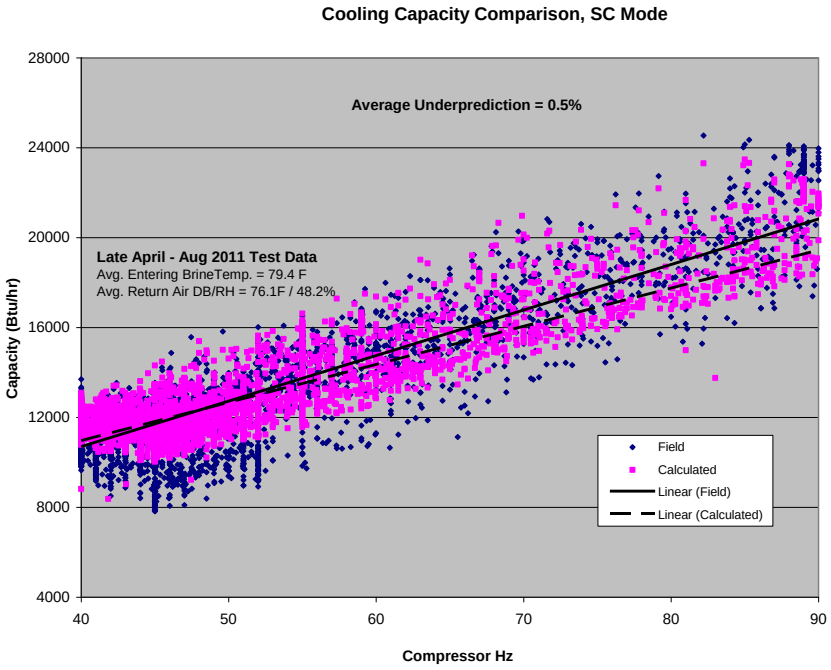

Figure 20. Space cooling capacity comparison between model and field versus compressor speed.

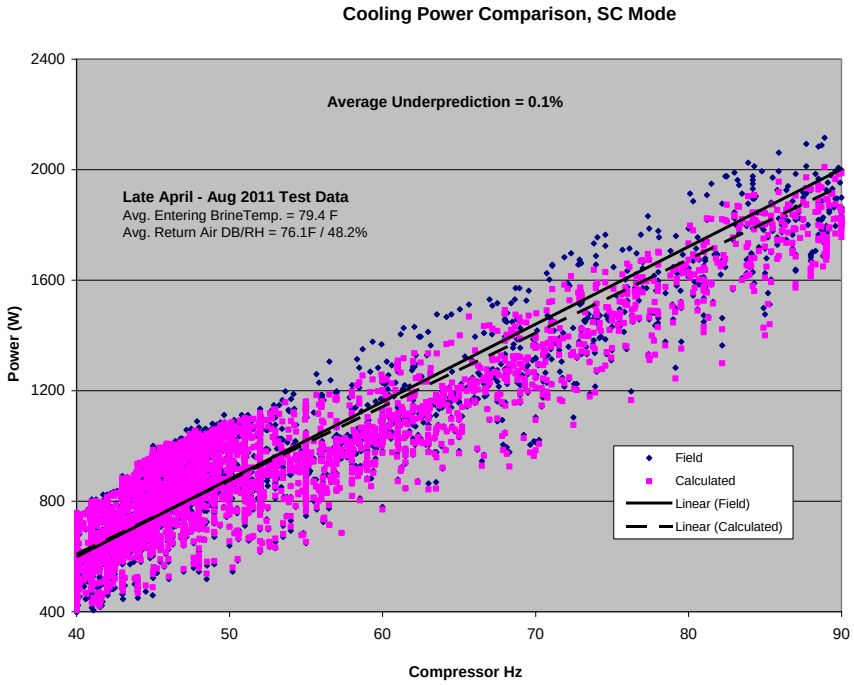

Figure 21. Space cooling power comparison between model and field versus compressor speed.

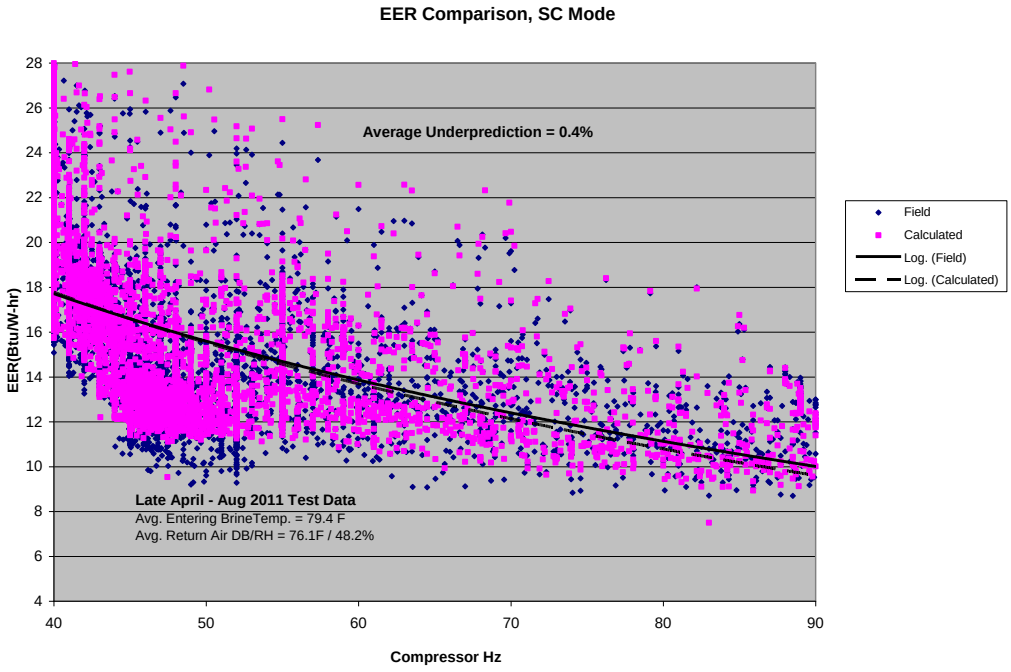

Figure 22. Space cooling EER comparison between fully adjusted model and field versus compressor speed.

3.3 Performance Comparisons for Combined Space Cooling and Water Heating Mode

Next, combined space cooling and water heating simulations were made using the 10 minute averaged compressor speeds and brine and DHW loop EWTs. As in dedicated WH mode, adjustments were made to match the measured DHW loop flow rates. Further adjustments were also made to match the compressor discharge temperatures and condenser exit subcooling levels.

Comparisons of space cooling and water heating capacity, total power, and combined EER are shown in figures 23-26. These are again plotted as a function of the compressor speed along with the average DHW EWT and indoor conditions. (The water heating set point was 120°F and the average EWT values varied only by 15ºF from min to max.) Here the agreements are much worse in delivered capacities and combined EER, but quite close in total power.
Average differences were 38.5% and 23.3% cooling and water heating capacities, within 0.1% in power, and 29.2% in combined EER.

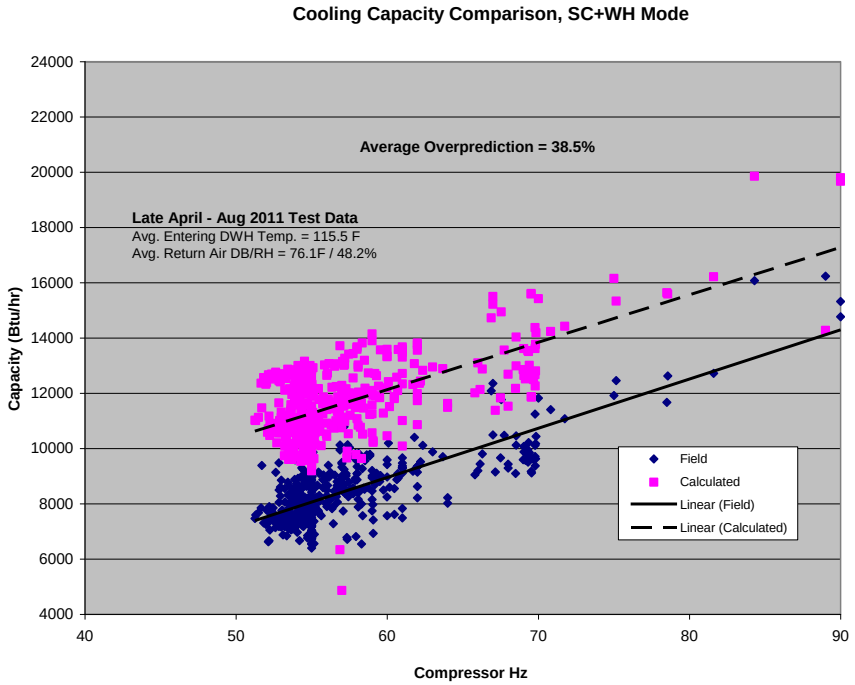

Figure 23. Space cooling capacity comparison in SC+WH mode between model and field versus compressor speed – based on indicated subcooling levels.

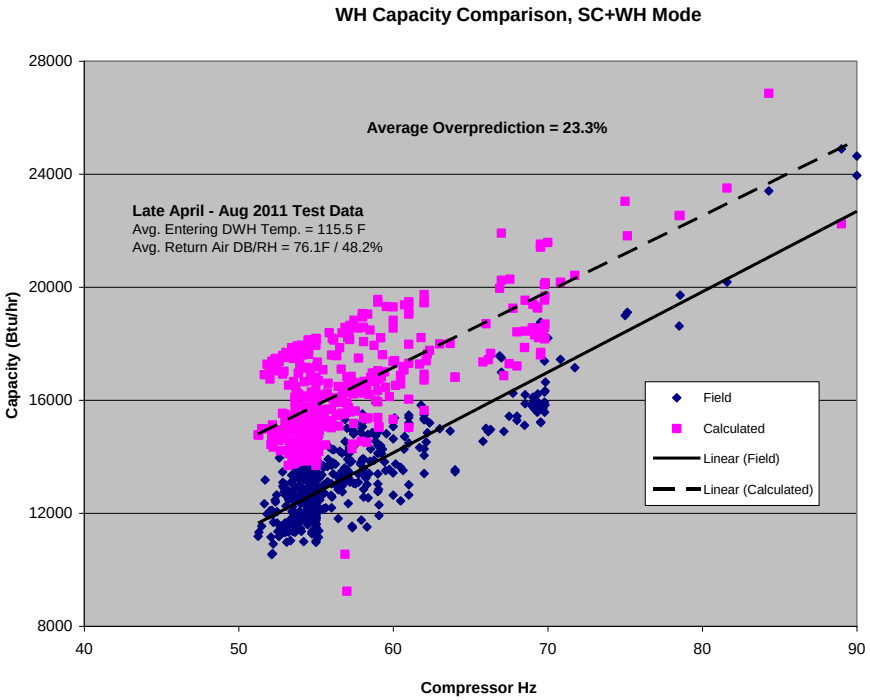

Figure 24. Water heating capacity comparison in SC+WH mode between model and field versus compressor speed — based on indicated subcooling levels.

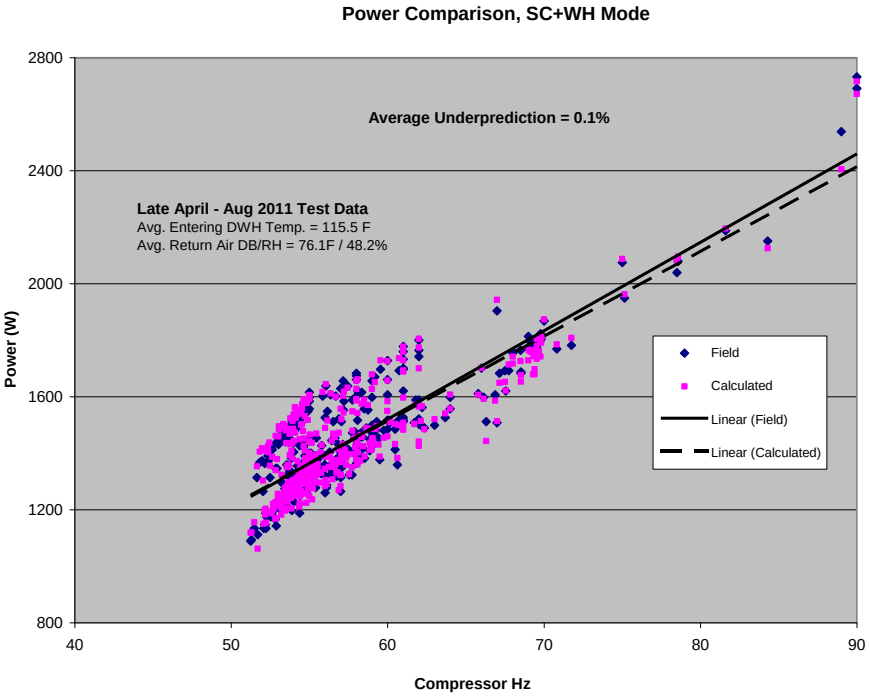

Figure 25. Power comparison in SC+WH mode between model and field versus compressor speed — based on indicated subcooling levels.

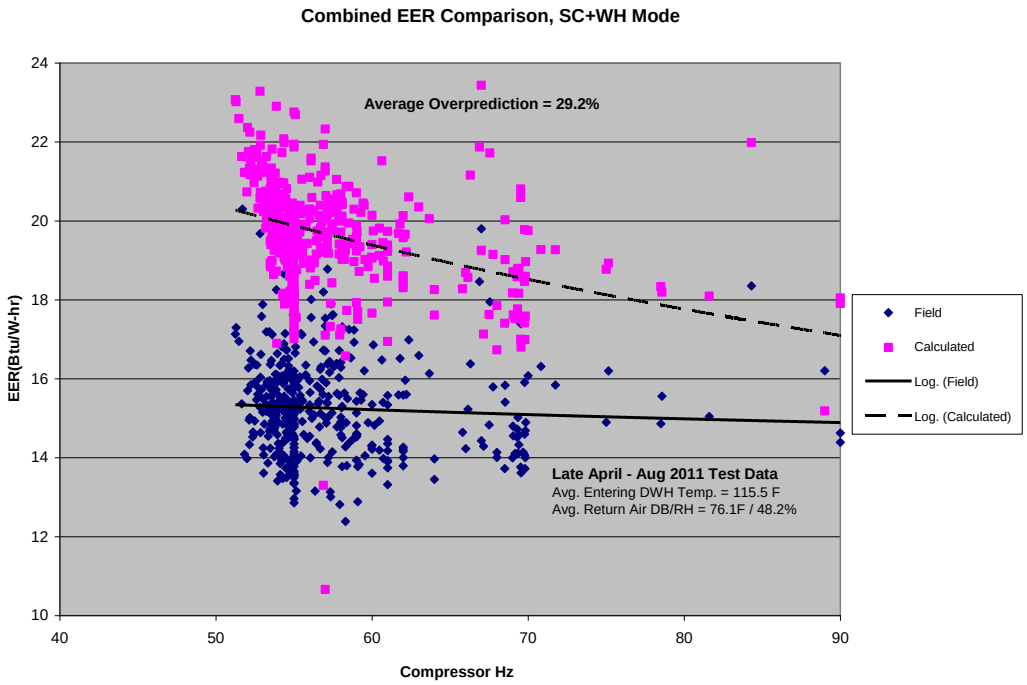

Figure 26. Combined EER comparison in SC+WH mode between model and field versus compressor speed — based on indicated subcooling levels.

3.4 Further Performance Comparisons for Combined Space Cooling and Water Heating Mode

Further investigation of these poorer agreements in the combined mode suggests that the unit was most likely operating significantly undercharged for the combined SC+WH mode. This is a valid possibility considering that the indicated subcooling levels were close to zero (averaging 0.4ºF) and that more charge is required in this mode than in the space cooling mode (with already low indicated subcooling levels averaging 1.8ºF as well); this is due to the 25% larger internal volume of the current DHW HX, relative to the brine HX. An energy balance on the refrigerant side using map-predicted refrigerant flow rates indicates that the actual exit conditions leaving the condenser may have had a leaving quality averaging 29%. Note that there is some uncertainty in the energy balance approach to calculating exit condenser conditions since there is some unknown amount of heat loss (presumably small) from the annular refrigerant side of the insulated DHW HX to the indoor section and in the water-side delta-T and flow measurements.

Additional HPDM simulations with these alternative exit condition values improved agreements on delivered capacities to within 10% on cooling capacity, 3.7% on water heating capacity, –4.6% on power, and 11.3% on combined EER, as shown in figures 27–30. The over-predictions appear consistent with under-predictions of the measured discharge saturation temperatures by about 3°F.

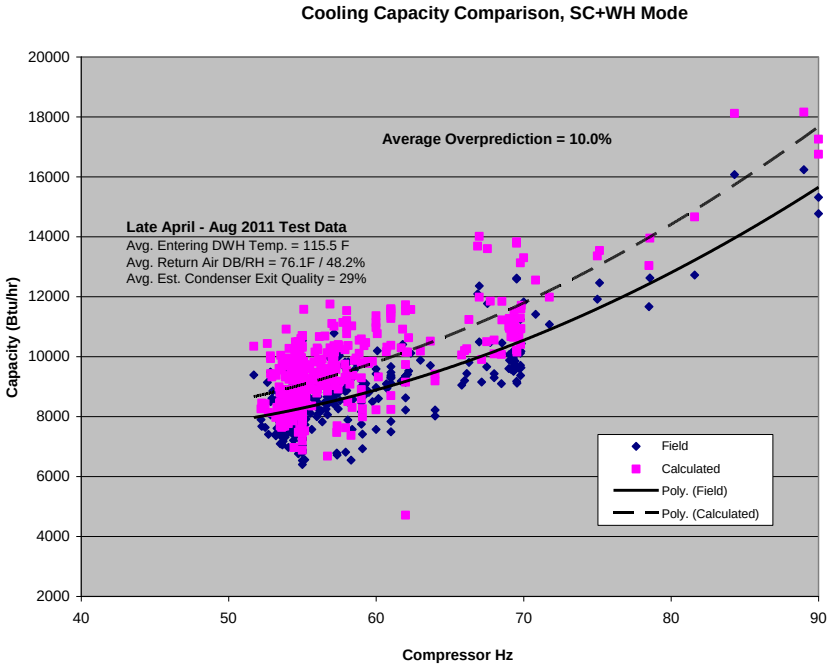

Figure 27. Space cooling capacity comparison in SC+WH mode between model and field versus compressor speed — based on calculated exit quality levels.

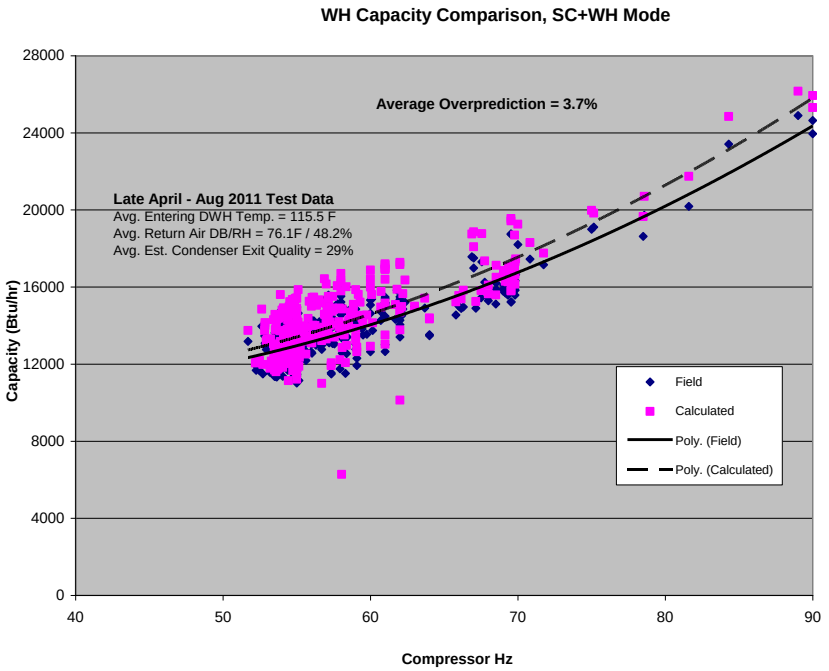

Figure 28. Water heating capacity comparison in SC+WH mode between model and field versus compressor speed — based on calculated exit quality levels.

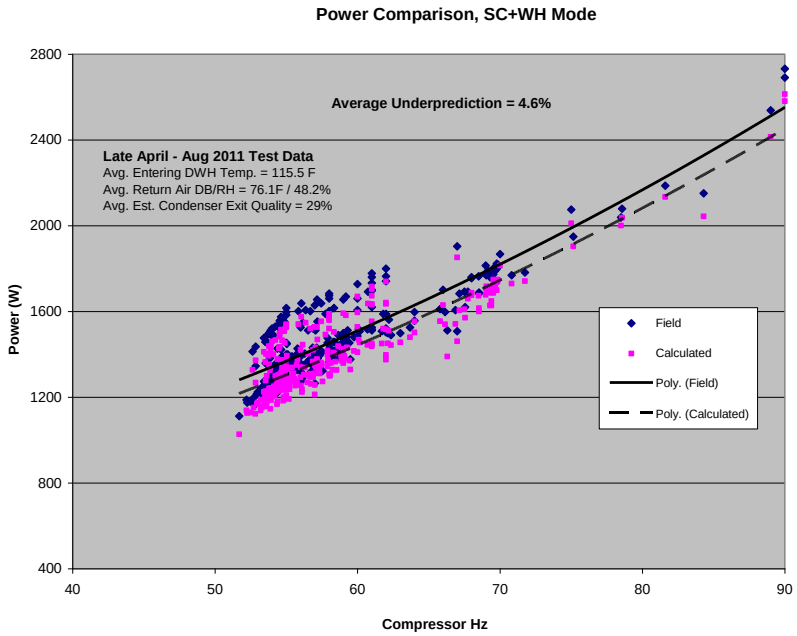

Figure 29. Power comparison in SC+WH mode between model and field versus compressor speed — based on calculated exit quality levels.

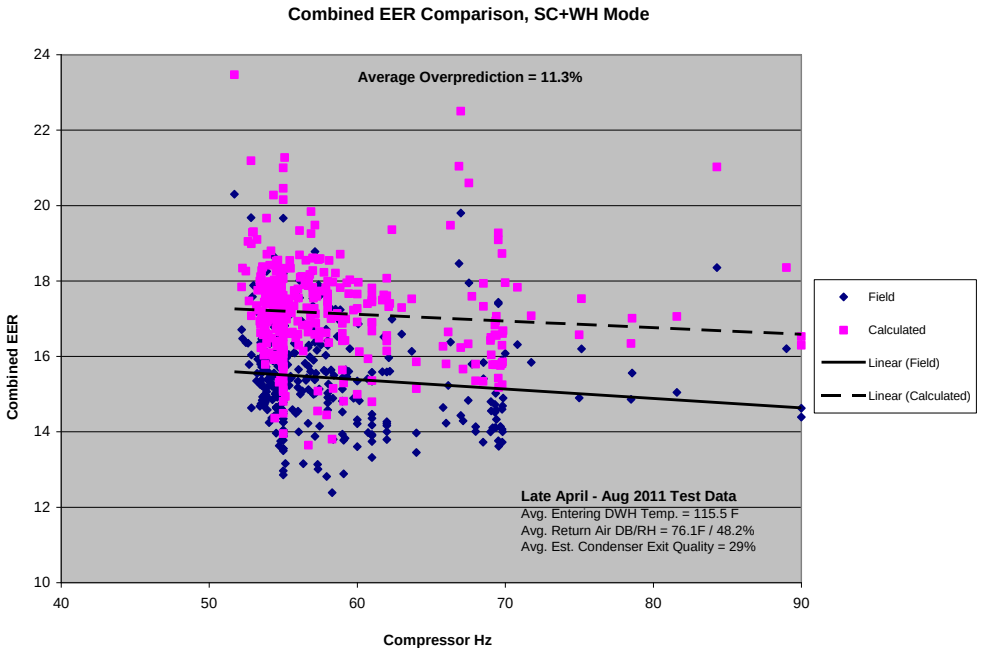

Figure 30. Combined EER comparison in SC+WH mode between model and field versus compressor speed — based on calculated exit quality levels.

3.5 Further Performance Comparisons for Space Cooling Mode

The low refrigerant charge indications found for the SC+WH mode led us to reexamine the exit condenser conditions for the SC mode based on the alternative refrigerant-side energy balance using map-based refrigerant flow rates. This analysis predicted that the exit condenser conditions in the SC mode were mostly two-phase with an average exit quality of 11%. Using these revised exit condenser conditions, our predicted SC performance agreements were –1.2%, –2.1%, and 1.0% for capacity, power, and EER, respectively. These average differences are slightly larger than those found earlier when using indicated subcooling values in figures 20–22, but still quite small. Figures 31–33 show the performance comparisons based on the alternative exit condition assumptions.

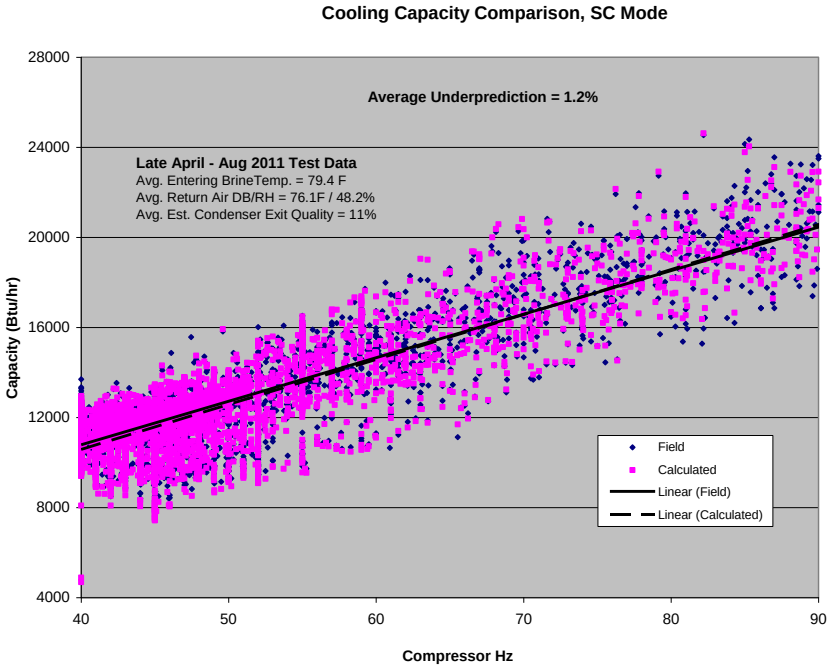

Figure 31. Space cooling capacity comparison between model and field versus compressor speed — based on calculated exit quality levels.

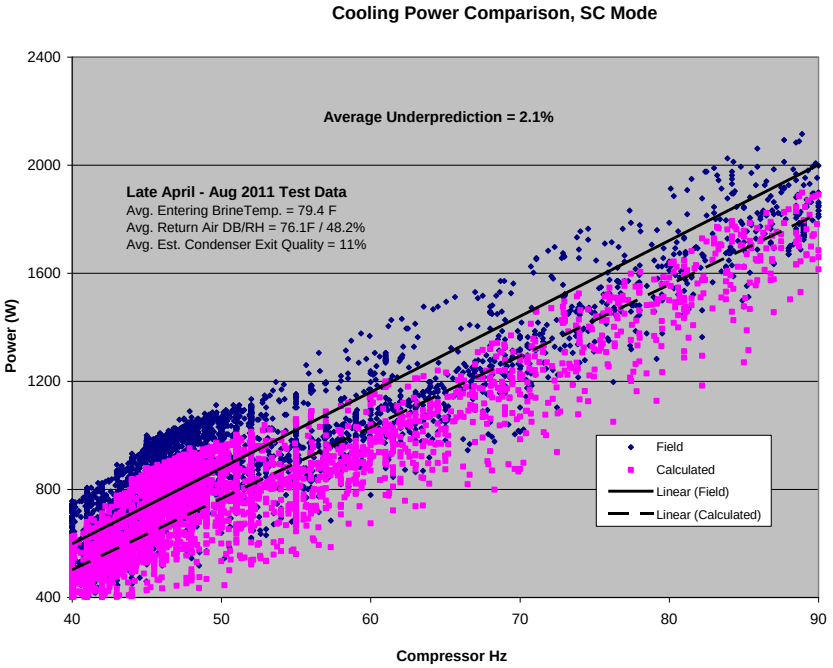

Figure 32. Space cooling power comparison between model and field versus compressor speed — based on calculated exit quality levels.

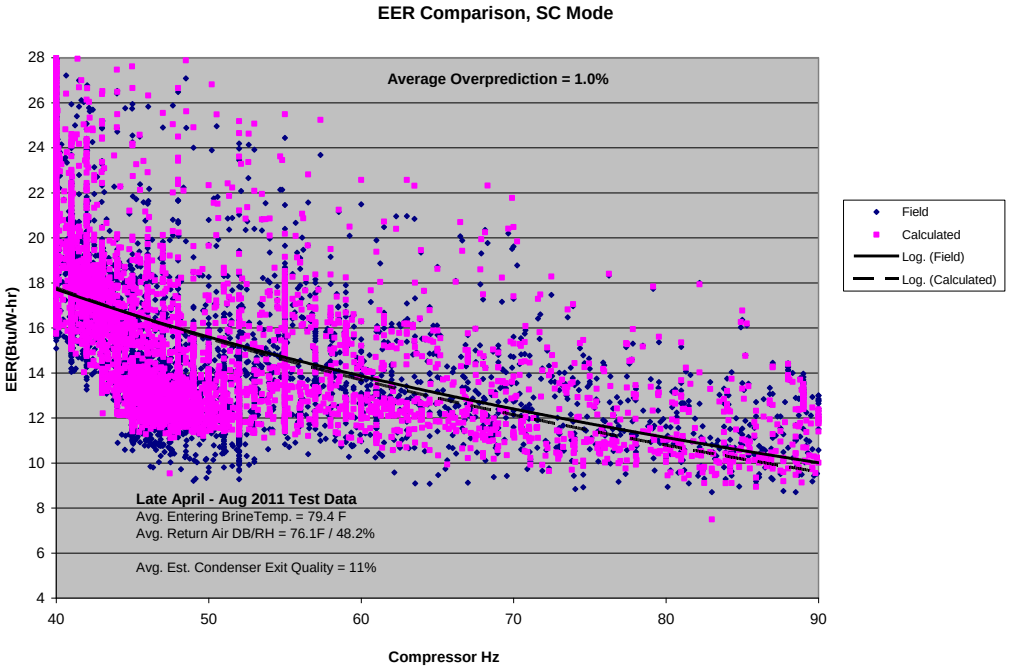

Figure 33. Space cooling COP comparison between model and field versus compressor speed — based on calculated exit quality levels.

4. FURTHER ANALYSIS OF WATER HEATING COMPARISONS IN HEATING SEASON

Next we revisited the dedicated WH results for the Jan–Feb tests reported earlier in this report. Using the alternative refrigerant-side energy balance, we calculated the exit condenser conditions and found an average indicated subcooling of 1.2°F, with a calculated quality up to 20% at some conditions, rather than the exit-temperature-measured, exit-pressure-estimated subcooling levels averaging 2.6°F. Using these alternative exit condenser conditions, new comparison runs were made with the HPDM. These results are shown below in figures 34–36 for WH capacity, power, and COP; average differences found from this approach were 3.1%, –4.4%, and 8.0%, respectively.

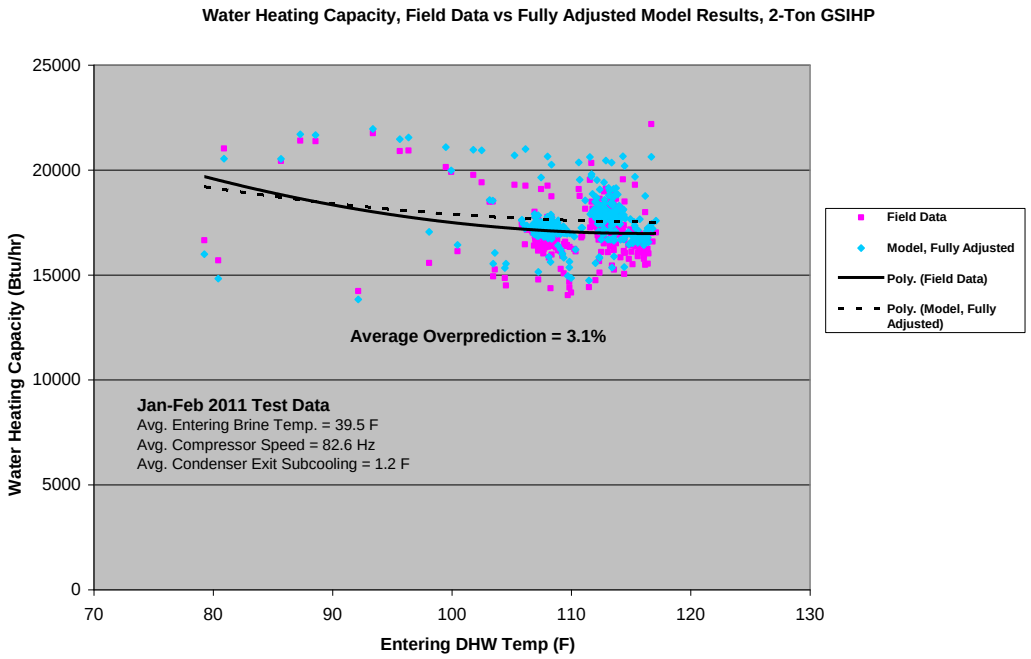

Figure 34. Water heating capacity comparison between model and field versus compressor speed — based on calculated exit quality levels.

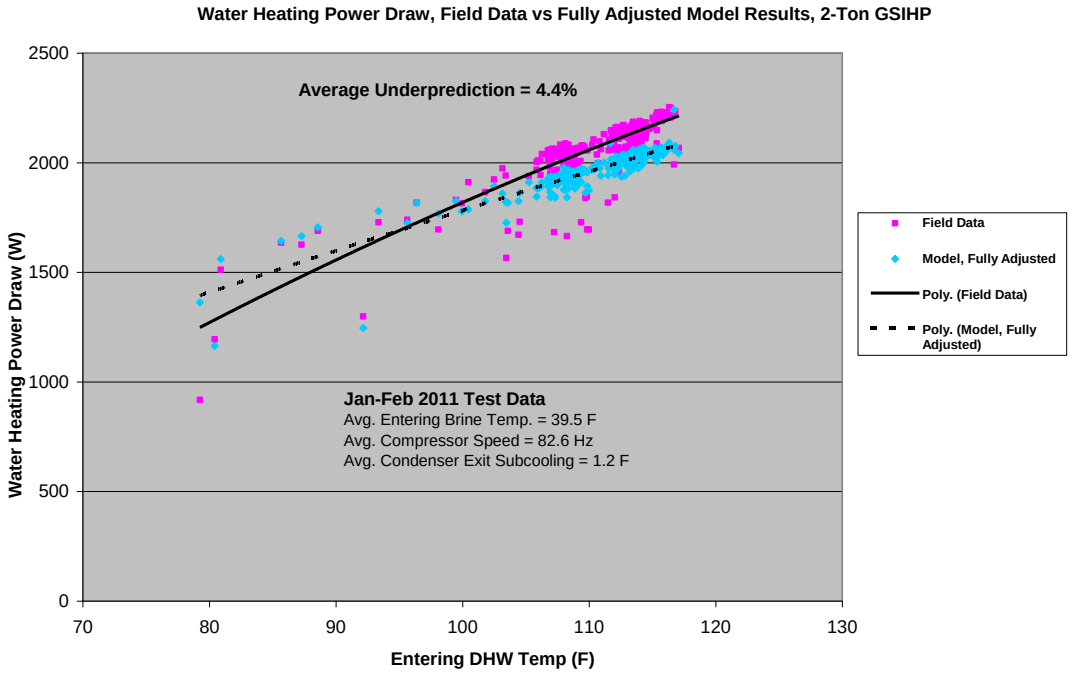

Figure 35. Water heating power comparison between model and field versus compressor speed — based on calculated exit quality levels.

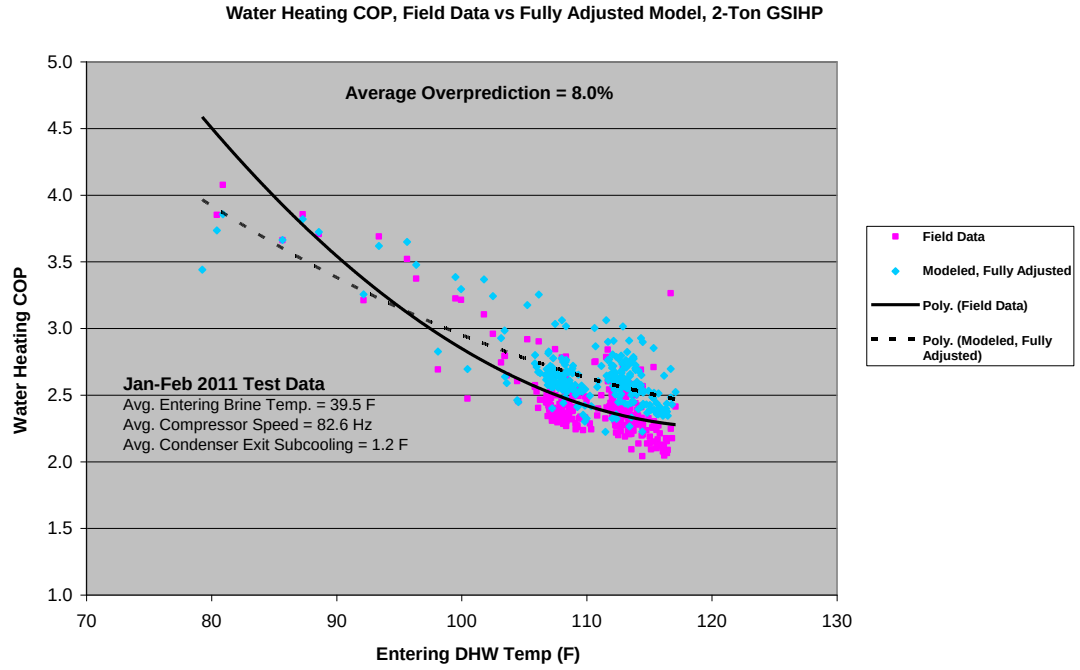

Figure 36. Water heating COP comparison between model and field versus compressor speed — based on calculated exit quality levels.

These differences in capacity are larger than predicted previously. However, for the second round of WH analysis, the measured water temperatures into and out of the DHW HX were revised based on later comparisons to a second set of water temperature measurements. This caused the average field-measured capacities to drop by 4.5%. This adjustment to the earlier modeled results would have given similar error levels. In either case, the model over-predictions are thought to be mainly because we are under-predicting the discharge saturation temperature by more than 4°F. This could be because in the lab water heating tests, the condensers were not well insulated. If there was significant heat loss in those tests, our HX calibration factors would likely be too high for the situation in the field test with well-insulated HXs, thus under-predicting the condensing temperatures.

Required system charge based on matching subcooling levels as measured in lab tests (and supported by the relative active and inactive HX internal volumes in the different modes) is highest for the SC+WH mode, with the dedicated WH mode next, followed by the space cooling mode, and finally space heating. Based on the similar results in the dedicated WH mode for the two approaches (after accounting for the later WH capacity field calculation correction) and measured subcooling levels between 3 and 20°F in SH mode, we determined that there was no need to make further comparisons in the SH mode. The close results for the two approaches in the WH mode and the large apparent level of undercharging in the SC and SC+WH modes also suggest that it is most likely that some refrigerant charge leaked from the system between the Jan –Feb heating season and the summer cooling season tests.

5. SUMMARY COMPARISON RESULTS

The following table summarizes the average differences by operating mode between the field data and the modeled results. The table contains results obtained using the measured subcooling levels as well as comparisons done using condenser exit conditions determined from energy balances. As noted earlier, agreements were improved for the SC+WH comparisons using the latter approach, due to the apparent low charge situation in this mode. However, the results for the WH mode obtained using the latter approach are poorer than those obtained using measured subcooling levels, primarily because of improved water temperature measurements after the space heating season which lowered the original field-indicated WH capacities by about 4.5%.

Table 1. Summary of average differences between the field-indicated and modeled capacities, total power, and efficiency

	Using measured subcooling levels				**Using condenser exit conditions determined from energy balances**		
% Difference	**SH**	**WH***	**SC**	**(SC+WH)**	**SC**	**(SC+WH)**	**WH**
SC or SC Capacity	–0.7		–0.5	38.5	–1.2	10.0	
WH Capacity		–1.3		23.3		3.7	3.1
Total Power	–1.6	–3.5	–0.1	0.1	–2.1	–4.6	–4.4
COP/EER	1.1	2.3	–0.4	29.2	1.0	11.3	8.0

*Before field-measured WH capacities were lowered by 4.5% in WH comparisons based on condenser exit conditions determined from energy balances and additional instrumentation.

6. CONCLUSIONS

The power draw from the variable-speed compressor is 10 to 20% lower than expected from the provided compressor maps at the lowest speed operation (35 to 40 Hz) in cooling mode. Up to 60 Hz operation, the power draw is still lower by 4 to 10% in space conditioning modes. The suction gas cooling of the inverter likely causes some change in the performance of the compressor–inverter combination from that measured by the manufacturer with an air-cooled inverter. Only in the space heating mode above 90 Hz are the measured compressor power levels higher than the manufacturer's map by 5 to 10%. Finally, the manufacturer tests are with a nominal airflow over the compressor, which is not the case in the actual installation with a separate indoor compressor and HX compartment. This would likely affect the compressor performance most in the space heating mode where the motor cooling per mass of refrigerant flow is the least.

The power draw from the indoor blower is also lower than expected due to the low resistance of the duct system in the field test. In contrast, the DHW pump power was higher than expected. The power draw from the brine loop pump was close to that assumed for a standard vertical well installation, even though this was a horizontal loop application.

From comparisons of performance in the four modes of operation, we conclude that the unit was most likely undercharged for some if not all of the time during the Jan–Sept 2011 test season.

After revising the modeling assumptions for the field input power relationships versus compressor speed or fluid flow and correcting for apparent undercharged condenser exit conditions, we found close agreement in space heating and cooling performance (±2%) for near-steady-state operating conditions. For cases in the space heating mode where the compressor speed is changing significantly from one time interval to the next, the agreements were worse, likely indicating that it is taking some time for new steady-state operating pressures to be established.

Agreements were not as close in the water heating modes, where the model over-predicted the WH capacity by 3.1 to 3.7% and water heating COP by 8 to 8.7%, while under-predicting total power use by 4.4 to 4.6%. Combined SC+WH EER was over-predicted by 11.3%

7. RECOMMENDATIONS

For future field tests of the GS-IHP unit, provisions should be made to ensure that full charge to the unit is provided and maintained. This would preferably be done by the manufacturer, as no field-installed refrigerant lines would be needed. If the internal volumes of the HXs are not changed in the upcoming prototype design, the combined SC+WH mode is the mode presently requiring the most charge (based on active internal volumes and highest condensing temperatures) followed by the dedicated WH mode. More than 3°F of subcooling in the SC+WH mode should be measured for an EHWT around 110°F and a compressor speed ≥70 Hz. In the dedicated WH mode, a subcooling near 10°F would be expected for EHWTs near 110°F and ≥70 Hz compressor speed. It is further recommended that the subcooling measurements in the test data be reviewed every month or two to confirm that the charge level has not gone down (as the added pressure gauges in the field test unit make refrigerant leaks more likely than in a production unit). This may be accomplished by using an energy balance on the condenser for

sample test periods to determine the exit state and checking this against the indicated subcooling level for major discrepancies. If the new prototype design has different internal volumes, then the subcooling recommendations should be revised based on lab data and calibrated models for the most charge sensitive operating modes.

If possible, it is recommended for future testing that the data acquisition system be reconfigured so that all data is collected with the same timestamp. This would avoid the data synchronization issues that had to be addressed in the FY11 data collection and reduction.

The discrepancies between the modeled and indicated indoor airflow in the heating mode suggest that the sensing of the supply air temperature may need to be improved.

A lower pressure drop flow meter could be considered for the DHW loop to reduce the pump power closer to design levels.

Further investigation is recommended to determine why we are generally under-predicting the field-indicated condensing saturation temperatures, especially in the water heating modes. New lab tests with well-insulated DHW HXs are recommended as well as further high-side energy balance analyses on the previous lab and field data.

We should account for equipment heat losses such as compressor and discharge line losses in the TRNSYS simulations for GS-IHPs where all the equipment is located indoors. This might be most conveniently done by adding an energy balance calculation in the TRNSYS calculations where the difference between the sum of the power inputs and the low-side energy input and the condenser output is added as heat to the house in an appropriate manner.

Going forward, we plan to use the field-calibration corrections and correlations for compressor, blower, and pump powers, manufacturer's control logic, and a full refrigerant charge assumption to develop GS-IHP performance maps to predict the potential annual performance in Wolf Creek House #2.

8. REFERENCES

Ally, M. R., J. D. Munk, V. D. Baxter, and A. C. Gehl. 2011. "Field Test of High Efficiency Residential Buildings with Ground-Source and Air-Source Heat Pump Systems," Paper # 00274, *10th IEA Heat Pump Conference*, Tokyo, Japan.

Murphy, R.W., V. D. Baxter, C. K. Rice, and W. G. Craddick. 2007. *Ground Source Integrated Heat Pump for Near Zero Energy Houses: Technology Status Report*. ORNL/TM-2007/177, December 2007.

Rice, C .K, Bo Shen, and J. D. Munk. 2011. "1st ClimateMaster Prototype, Predicted Energy Savings,GSIHP CRADA," presentation to ClimateMaster by ORNL, December 2011.

APPENDIX: UNCERTAINTY ANALYSIS ON CAPACITY AND POWER DETERMINATIONS FROM FIELD MEASUREMENTS

The manufacturer's specified accuracy on the flow meter is ±1.5% of the indicated rate. The brine temperatures measured in the cooling season have an accuracy and interchangeability of ±0.27°F and a linearity deviation of ±0.12°F.

Energy delivered for space cooling (SC)

$$Q_{Cool} = V_{brine}\rho_{brine}c_{p,brine}\Delta T_{brine} - E_{Total}$$

Uncertainty for SC Capacity

$$u_Q = \sqrt{\left(\frac{\partial Q}{\partial V}u_V\right)^2 + \left(\frac{\partial Q}{\partial \Delta T}u_{\Delta T}\right)^2 + \left(\frac{\partial Q}{\partial E}u_E\right)^2}$$

$$u_Q = \sqrt{\left(\rho_{brine}c_{p,brine}\Delta T u_V\right)^2 + \left(V_{brine}\rho_{brine}c_{p,brine}u_{\Delta T}\right)^2 + (u_E)^2}$$

$$u_{\Delta T} = \sqrt{u_{T,in}^2 + u_{T,out}^2}$$

Uncertainty in SC is 7.6% ignoring any uncertainty in the brine concentration.

Uncertainty for SC including ±5 percentage points uncertainty in propylene glycol concentration by volume

$$u_Q = \sqrt{\left(\rho_{brine}c_{p,brine}\Delta T u_V\right)^2 + \left(V_{brine}\rho_{brine}c_{p,brine}u_{\Delta T}\right)^2 + (u_E)^2 + \left(V_{brine}c_{p,brine}\Delta T u_\rho\right)^2 + \left(V_{brine}\rho_{brine}\Delta T u_{c_p}\right)^2}$$

Capacity uncertainty in SC is 7.9% including the effect of uncertainty in the brine concentration.

Energy delivered for water heating (WH)

$$Q_{WH} = V_w\rho_w c_{p,w}\Delta T_w$$

Uncertainty for WH Capacity

$$u_{Q,WH} = \sqrt{\left(\rho_w c_{p,w}\Delta T_w u_V\right)^2 + \left(V_w\rho_w c_{p,w}u_{\Delta T}\right)^2}$$

Uncertainty in WH capacity is 5.3%.

Energy delivered for SC while in SC+WH mode

$$Q_{SC} = V_w \rho_w c_{p,w} \Delta T_w - E_{Total}$$

Uncertainty for SC while in SC+WH mode

$$u_{Q,SC} = \sqrt{(\rho_w c_{p,w} \Delta T_w u_V)^2 + (V_w \rho_w c_{p,w} u_{\Delta T})^2 + u_E^2}$$

Uncertainty in SC is 8.1% while in combined SC+WH mode.

Heating capacity measurement uncertainty is undetermined due to issues discovered at the end of the heating season with the entering brine temperature sensor.

The energy use measurements consist of a current transformer (CT) and WattNode. The accuracy on the CT is ±1%. The accuracy of the WattNode is ±0.5% of the reading.

$$u_E = \sqrt{u_{CT}^2 + u_{WN}^2}$$

Uncertainty in power measurements was 1.1%.